



# The impact of peripheral circulation characteristics of typhoon on sustained ozone episodes over the Pearl River Delta region, China

Ying Li<sup>1,2</sup>, Xiangjun Zhao<sup>1,2,3\*</sup>, Xuejiao Deng<sup>4\*</sup>, Jinhui Gao<sup>1,2,5</sup>

<sup>1</sup> Department of Ocean Sciences and Engineering, Southern University of Science and Technology, Shenzhen, China

<sup>2</sup> Southern University of Science and Technology, Shenzhen, China

<sup>3</sup> School of Mathematics and Finance, Chuzhou University, Anhui 239000, China

<sup>4</sup> Institute of Tropical and Marine Meteorology/Guangdong Provincial Key Laboratory of Regional Numerical Weather Prediction, China Meteorological Administration, Guangzhou, China

<sup>5</sup> Plateau Atmosphere and Environment Key Laboratory of Sichuan Province, School of Atmospheric Sciences, Chengdu University of Information Technology, Chengdu, China.

\* Corresponding author e-mail address: (iamzxj841025@163.com) and (dxj@gd121.cn)

**Abstract.** It is widely reported that the peripheral circulation of typhoon favors for the formation of sustained ozone episodes. However, the process how it impact on the day-to-day ozone pollution levels during the episodes have not been clearly studied. Which is crucial for better prediction of the daily ozone variation. In this study, the analysis of ground observation, wind profile data, and model simulation are integrated. By analyzing the wind profile radar observations, we found a weak winds deepening (WWD; vertical depth of the weak winds increased), which is more correlated to the ground-level ozone variation than surface weak wind. Long-term statistical analyses show that the WWD is a common weather phenomenon that occurs in the peripheral subsidence region of typhoons and was generally accompanied by ozone pollution episodes. WRF-Chem with process analysis simulation show that under the impact of the peripheral subsidence chemical formation (CHEM) and vertical mixing (VMIX) effects are two major contributors to the enhancement of ozone levels, while the advection (ADV) are always negative values. But regarding the daily variability of the daytime ozone levels during the episode, it do not determined by the daily variation of daytime CHEM and VMIX, but that of the ADV term. A detail day-to-day analysis show that weak subsidence associated with typhoon periphery provide the premise for the clear sky and warmer air, which is conducive for the ozone photolysis formation (CHEM) above the ground in planetary boundary layer (PBL) and compensate the ozone through the positive VMIX effects on the ground. The WWD induced by the peripheral circulation of typhoon system provide the premise for the day-to-day positive contribution of ADV term to ozone enhancement throughout the whole planetary boundary layer (PBL), which play an important role in determining the day-to-day daytime ozone variation. These results indicate the important role of the WWD in the lower troposphere for the formation of sustained ozone episodes due to the peripheral circulation of the typhoon, which helps to better predict the daily changes of daytime ozone levels.



## 32 1. Introduction

33 The Pearl River Delta (PRD) located in the coastal region of South China, which is often affected by typhoon  
34 systems, has experienced major economic development and urbanization in the past two decades, and has been  
35 accompanied by large increases in air pollution and decreases in visibility (Wang et al., 1998, 2001; Lai and Sequeira,  
36 2001). Ozone pollution is the most important air pollution issue in this region; ozone has been the ‘primary pollutant’  
37 since 2014 (Ministry of Ecology and Environment of China, 2016). Ozone is harmful to human health and has adverse  
38 effects on vegetation and crops, among others (Aunan et al., 2000; Felzer et al., 2007; Feng et al., 2015). Ozone  
39 concentrations are determined by the photochemical reactions of its precursors and by the local meteorological  
40 conditions. However, ozone pollution episodes are mainly triggered by weather conditions rather than by sudden  
41 increases from emission sources (Ziomas et al., 1995; Giorgi and Meleux, 2007; Lin et al., 2019).

42 The Guangdong Haze Weather Bulletin (Wang, 2017) has classified the weather patterns affecting regional pollution  
43 events into cold fronts, cold high-pressure systems moving towards the sea, uniform pressure fields, Western Pacific  
44 subtropical high (WPSH), tropical cyclone (TC) peripheries, and weak cold high-pressure ridges. By using observational  
45 data, several studies have reported the impacts of TC activity on meteorological factors that are favourable for air  
46 pollution over the PRD region (Feng et al., 2007; Chen et al., 2008; Wu et al., 2013). TCs are typical weather systems that  
47 are responsible for both high ozone and PM<sub>2.5</sub> pollution over the PRD (Chen et al., 2008; Deng et al., 2019).

48 Many studies in the PRD region and other coastal regions of China have shown the significant impact of TCs on  
49 forming ozone (TCs-Ozone) episodes in recent years (Zhang et al., 2012; Li et al., 2013, 2014; Zhang et al., 2013; Jiang et  
50 al., 2015; Huang et al., 2015; Shu et al., 2016, 2019; Tan et al., 2018; Chen et al., 2018; Han et al., 2019). TCs-Ozone  
51 episodes generally occur when weather conditions include high temperatures, radiation flux, low relative humidity, and  
52 weak winds (Cheng et al., 2016; Liu et al., 2017). There were large amount of observational-based studies reporting the  
53 TCs-Ozone episodes are weak wind related, however it is very few about the study of the influence mechanism of weak  
54 wind on ozone in TCs-Ozone episodes. In addition, previous integrated process rate (IPR) analysis based on numerical  
55 modelling simulations have reported that the chemical (CHEM) and vertical mixing (VMIX) effects are two major



56 contributors to ozone episodes, whereas advective transport (ADV) is generally a consumptive process(Shu et al., 2016;  
57 Wang et al., 2009). The inconsistencies between observational and simulated results of wind contributions to ozone  
58 episodes are poorly understood, which may be due to the lack of studies of influence mechanism of weak wind on ozone  
59 concentration enhancement.

60 In addition, for the air quality forecast and prevention, it is more important to understand the mechanism leading to the  
61 day-to-day variation of the daytime ozone levels, since the ozone levels always reach its peak values in the daytime due  
62 to photo-chemistry and ozone converted to NO<sub>2</sub> temporarily in the absence of light incidents at nights. However, though  
63 the TCs-Ozone episodes have been widely reported, the studies of mechanism on the daily daytime variation of during  
64 sustained TCs-Ozone episodes are quite limited.

65 Thus, the objective of this study is **to the impact** processes of typhoon circulation characteristics on the day-to-day  
66 variation of daytime ozone concentration in TCs-ozone episode. The analysis of ground observation, wind profile data,  
67 and WRF-Chem model simulation with process analysis are integrated. Detailed data and model description are  
68 provided in Sect. 2, followed by the results and discussion in Sect. 3. The last section summaries the main conclusions.

## 69 **2. Data and model**

### 70 **2.1 Data**

71 In this study, hourly surface ozone concentrations from 2016 over mainland China were obtained from the Ministry of  
72 Environmental Protection of China. The 3D wind profiler data, automatic weather station data, cloud data, and solar  
73 radiation measurements were provided by the China Meteorological Administration and were used for the  
74 meteorological analyses of Typhoon Nepartak. The Final (FNL) Operational Global Analysis data that were used to  
75 describe the circulation of Typhoon Nepartak have a horizontal resolution of 1° x 1° with 27 vertical levels and were  
76 obtained from the National Centers for Environmental Prediction(NCEP), USA .

77 The observations of a typical ozone episode occurred in the PRD region during 7–10 July 2016 (local standard time; LST)  
78 before Typhoon Nepartak made landfall was collected and deeply analyzed . Typhoon Nepartak intensified into a super



79 typhoon at 20:00 on 5 July, then gradually moved northwest due to the forcing of the WPSH over its northeastern side  
 80 (Fig. S2). At 05:50 on 8 July, the typhoon made landfall in Taitung County, Taiwan, with a maximum wind speed of 60 m  
 81  $s^{-1}$ , and again in Shishi City, Fujian at 14:00 on 9 July, with a maximum wind speed of 23  $m s^{-1}$ . At 03:00 on 10 July, the  
 82 typhoon weakened into a tropical depression.

83

## 84 2.2 Model descriptions

85 WRF-Chem is a widely used and fully coupled online 3D Eulerian chemical transport model  
 86 (<https://ruc.noaa.gov/wrf/wrf-chem/>) that considers both chemical and physical processes(Zhang et al., 2010; Forkel et  
 87 al., 2012); version 3.9.1.1 was applied in this study. Detailed descriptions of the meteorological and chemical aspects of  
 88 the WRF-Chem model can be found in Grell et al.(2005) and Skamarock et al.(2008). For the simulation, two nested  
 89 domains (Fig. S1) were set up with horizontal resolutions of 27 and 9 km and grids of  $283 \times 184$  and  $223 \times 163$  for the  
 90 parent domain (D1) and nested domain (D2), respectively. D1 was centred at (28.5°N, 114.0°E) covering most of China,  
 91 the surrounding countries, and the ocean. Corresponding simulations provided meteorological and chemical boundary  
 92 conditions for D2, which covered most of southern China.

93 There were 39 vertical layers that extended from the surface up to a pressure maximum of 50 hPa, 12 of which were  
 94 located in the lowest 2 km to fully describe the vertical structure of the PBL. Carbon Bond Mechanism Z (CBM-Z),  
 95 which includes 133 chemical reactions for 53 species and extends the model framework to function for a longer time  
 96 period and at a larger spatial scale than its predecessor, was used as the gas-phase chemical mechanism(Zaveri and Peters,  
 97 1999). The corresponding aerosol chemical mechanism was the Model for Simulating Aerosol Interactions and  
 98 Chemistry (MOSAIC) with eight bins(Zaveri et al., 2008), which is extremely efficient and does not compromise  
 99 accuracy of the aerosol model calculations. Other major model configuration settings are listed in Table 1.

100 **Table 1.** Major model configuration options used in the simulations.

ITEM	Selection
Long wave radiation	RRTMG
Shortwave radiation	RRTMG
Microphysics scheme	Lin scheme



Boundary layer scheme	Yonsei University (YSU) scheme
Land surface option	Noah land surface model
Photolysis scheme	Fast-J photolysis
Dry deposition	Wesely scheme

### 3. Results and discussion

#### 3.1 Episodic data analysis

The ozone pollution level and the meteorological conditions of the typhoon Nepartak case was first analyzed. As shown in Fig. 1, Guangdong province experienced a severe ozone pollution during the period. 28% (7 July) to 57% (10 July) of the air quality stations in Guangdong Province exceeded the national air quality standard level-II for ozone ( $200 \mu\text{g m}^{-3}$ ) at the daily peaks (16:00 LST). To show the vertical motion of the typhoon centre and peripheral region, we constructed a cross section through the typhoon system (points A and B; Fig. 2a-d) and plotted the corresponding vertical velocities (Fig. 2e-h) using the NCEP data. As shown in Fig. 2e-f, the western subsiding branches of vertical typhoon circulation were located over the PRD during 7–8 July, when ozone concentrations increased significantly compared to those of 6 July. After Typhoon Nepartak made landfall at Shishi City on 9 July, the peripheral subsidence had moved to the western area of the PRD region (Fig. 2g–h) and the PRD region was influenced by weak vertical motion and a weak horizontal wind field. Peak ozone levels exceeded 100 ppb at most of the monitoring stations in the PRD at this time. On 11 July, Typhoon Nepartak dissipated and the surface ozone concentrations began to decrease (Fig. 1f).

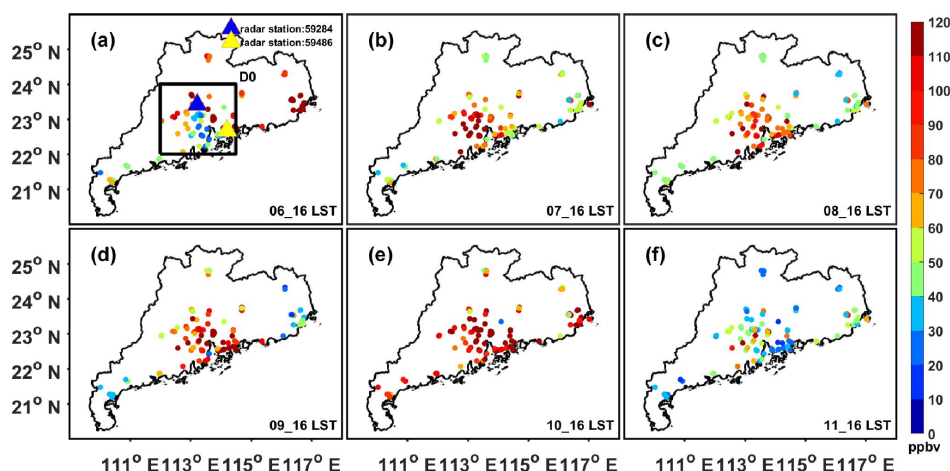
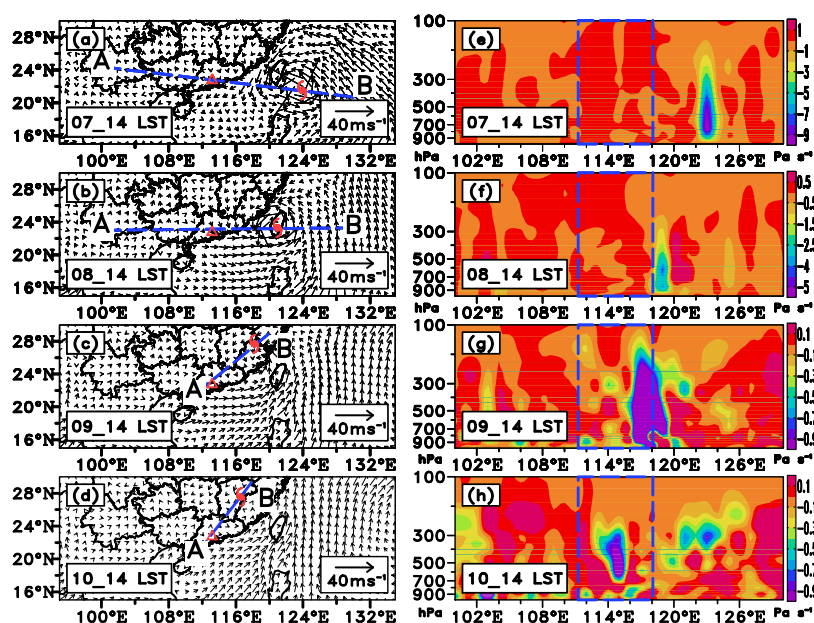


**Figure 1.** The horizontal distribution of surface ozone concentration over PRD at 16:00 from (a) 6 July 2016 to (f) 11 July 2016. The yellow



116 and blue triangles in (a) denote the positions of wind profiler station 59486 and 59284. The black box D0 indicates the area where the severe  
 117 ozone pollution event occurred.



118  
 119 **Figure 2.** (a)-(d) 1000 hPa wind vectors of NCEP-FNL data from 14:00 7 July to 14:00 10 July with red triangle and typhoon signs  
 120 representing PRD center and Nepartak locations, respectively. (e)-(h) vertical cross sections of vertical velocity along the four straight lines  
 121 linking PRD and the centers of Typhoon Nepartak in (a)-(d) from 14:00 7 July to 14:00 10 July 2016. The four blue dashed boxes denote the  
 122 longitude range of PRD in (e)-(h).

123 The weather over the PRD region was characterized by clear sky, strong solar radiation (Fig. 3a), low relative humidity  
 124 (Fig. 3b), and high temperatures (Fig. 3c), when the subsiding branches of vertical typhoon circulation were located over  
 125 the PRD during 7–8 July (Fig. 2e-f). The variations in these surface meteorological variables exhibited favorable  
 126 conditions for increasing ozone concentrations (Cheng et al., 2016; Liu et al., 2017). However, the height of the PBL  
 127 increased significantly on 8 and 9 July (Fig. 3c), and the atmosphere was under unstable conditions, which was indicated  
 128 by the overlapping temperature soundings and the parcel traces below 800 hPa (Fig. 3d–f). This instability is also shown  
 129 by the large values of convective available potential energy (CAPE; Fig. 3d–f), which is another criterion used to  
 130 determine the stability of atmosphere. In general, when the CAPE is  $\sim 1000 \text{ J kg}^{-1}$ , the atmosphere is unstable, which is  
 131 favorable for convection. These results illustrate that, under the control of typhoon periphery, the PBL height can be  
 132 increased in unstable atmospheric conditions, which is opposite from the observations in some TCs-haze events (Wu et



al., 2005 and Feng et al., 2007). For example, the research of Wu et al.(2005) reported that the TC produces a strong descending motions in the lower troposphere, a weak surface wind speeds, and a lower PBL. As a result, the strong peripheral subsidence of TC causes descending air motions to force the aerosol particles into a very shallow layer, and the weak horizontal winds keep the pollutant aerosols inside the source region, resulting in very high concentrations. Our observational results indicate that the TCs-Ozone episodes are not dependent on the enhancement of atmospheric thermal-dynamical stability and reduction of the PBL.

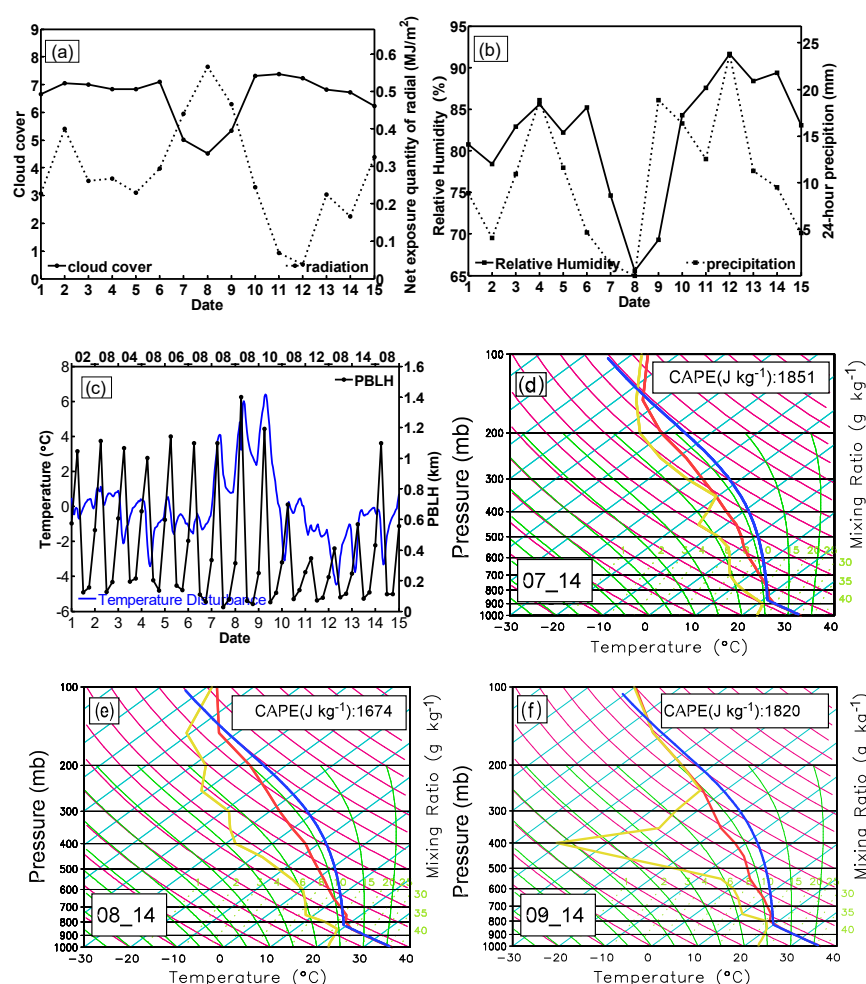


**Figure 3.** Time series of diurnal mean (a) cloud cover, radiation at 59287 observation station, (b) relative humidity, 24-h precipitation and averaged (c) PBLH and temperature anomaly of region D0 from 1 to 15 July; The SkewT/LogP at 14:00 on 7 July (d), 8 July (e) and 9 July (f); the solid thick red, blue and yellow lines in d,e and f denote the temperature sounding, the parcel path from surface upward and the parcel path from surface upward and the parcel path from surface upward.





dewpoint sounding, respectively.

The evolution of the vertical profile of horizontal winds at representative station 59284 is shown in Fig. 4a. Before 5 July, the wind speed was increasing with the vertical atmospheric layers. There were relatively larger wind speeds above the PBL and relatively weaker wind speeds below  $\sim 700$  m, with relatively low surface ozone concentrations ( $<40$  ppbv). On 5 July, the daily ozone concentration started to increase ( $>70$  ppbv) as the depth of WWD increased simultaneously. The depth of WWD was  $\sim 3$  km during 7–9 July with a sustained increasing ozone peak. On the night of 11 July, the horizontal wind speed above  $\sim 1$  km increased significantly and the ozone concentration decreased sharply. Variations in the wind profile and surface ozone at another representative station are also shown in Fig. 4b. At this station, the depth of WWD started to increase on 7 July, with a gradually increasing ozone peak value. Co-variations of the ozone concentration and WWD at other radar stations were also observed (Fig. S3–5). This co-variation is not a local effect, but is instead a regional phenomenon.

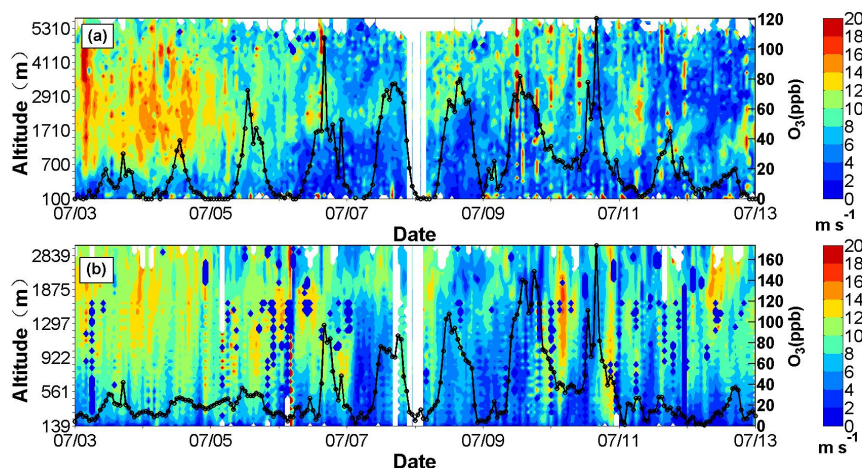


**Figure 4.** The profile evolution of horizontal wind speed from 3 to 13 July. the black solid lines are the surface ozone concentrations at (a) 59284 and (b) 59486 wind profile radar station.

By analyzing the wind profile data (Fig. 4), we noticed that the vertical depth of the horizontal weak wind generally increased from the surface up to the lower troposphere ( $\sim 2$ – $3$  km) and the surface ozone concentration changed with the change of vertical depth of the horizontal weak wind. To further illustrate the different impact of the surface weak wind and the WWD on surface ozone concentrations, the correlation coefficients between the surface ozone concentrations





and the average wind speeds from surface to different altitudes (up to 6 km) at different radar stations were calculated (Fig. 5). The correlation coefficients show an increasing trend with altitude, reach their maximum values between 2–3 km and remain stable above ~2.5 km. The average correlation coefficient at the surface was 0.57 (0.41–0.67) and the average correlation coefficient above 2000 km was ~0.75 (0.69–0.83) for seven radar stations. This indicates the potential impact of WWD on the ozone pollution episode induced by Typhoon Nepartak.

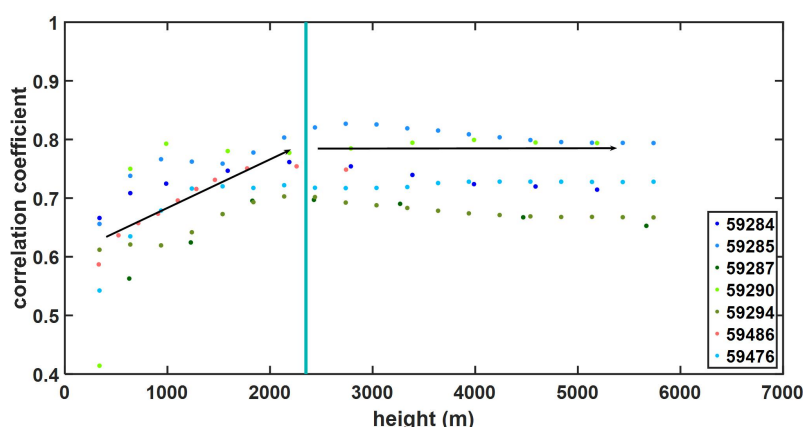


**Figure 5.** Correlation coefficient between the evolution of average wind speed and the evolution of ground ozone concentration in different altitude ranges of each wind profile radar station.

### 3.2 Long-term statistical analysis of the relationship between WWD and the O<sub>3</sub> episode

The above observational analysis shows that there was no stable atmospheric stratification and a decrease in the height of the boundary layer in this ozone pollution episode. The analysis of wind profile radar data and the correlation coefficients between the surface ozone concentrations and the average wind speeds between the surface and the altitude of each vertical layer (up to 6 km) indicate that in this episode of ozone pollution, WWD may have played an important role in the increasing of ozone pollution at the surface. Guangdong Province is located on the western coast of the Pacific Ocean and is frequently affected by typhoons annually. To investigate whether the relationship between WWD and ground-level O<sub>3</sub> only occurred in this case study or is a common phenomenon, a long-term statistical analysis of historical data was conducted. A statistical analysis of tropical cyclone wind fields in the Northwestern Pacific Ocean from 2014 to 2018 (based on Guangdong wind profiler data) was conducted. As not all the radar stations in Guangdong province are available during a typhoon, the available statistics number of each radar station for the 38 typhoons were



recorded as M. The number of WWD instances at each radar station was recorded as n. Ozone concentrations above 100  $\mu\text{g m}^{-3}$  are harmful to human health (Organization, 2005). The PRD regional background ozone concentration is generally less than 80–100  $\mu\text{g m}^{-3}$  and the ozone concentrations at most stations can exceed 160  $\mu\text{g m}^{-3}$  (national AQ standard Level-I) during a regional ozone pollution event. Therefore, ozone concentrations of 100–160  $\mu\text{g m}^{-3}$  and above 160  $\mu\text{g m}^{-3}$  were used to denote regional light and heavy ozone pollution in the statistics. The numbers of regional light and heavy ozone pollution events at each radar station were recorded as n1 and n2, respectively. As shown in Table 2, the number of WWD occurrences (n) accounts for 87–97% of the available number (M) of radar stations in the 38 typhoon statistics for the seven radar stations. The average value of n/M for the seven radar stations is 93%. This indicates that, when there is a tropical cyclone in the Northwestern Pacific Ocean, WWD will occur in whole or part of Guangdong province. The number of ozone pollution occurrences (n1+n2) accounts for 78%–100% of the number of WWD occurrences (n). The average value of (n1+n2)/n for the seven radar stations is 94%. The above statistical results show that WWD may be a common phenomenon on the periphery of typhoons and is often accompanied by significant increases in ozone concentrations.

Table 2. The statistical results of the peripheral weak wind of 38 tropical cyclones for 7 radar stations in Guangdong

Province and ozone concentration from 2014 to 2018.

Radar station number	n/M	(n1 + n2)/n
59294	33/38 (87%)	(21+11)/33 (97%)
59486	32/33 (97%)	(18+12)/32 (94%)
59476	29/30 (97%)	(22+5)/29 (93%)
59285	33/36 (92%)	(21+12)/33 (100%)
59287	35/38 (92%)	(23+12)/35 (100%)
59284	24/25 (96%)	(19+5)/24 (100%)
59290	28/30 (93%)	(13+9)/28 (78%)
Ave.	93% (87%–97%)	94% (78%–100%)

197



198 The above correlation coefficients and statistical analysis indicate that WWD may be a common weather phenomenon  
199 in the periphery of typhoon and could play an important impact on the ground-level ozone concentration. Therefore, the  
200 following attempts to give the influence mechanism of WWD on ground-level ozone pollution and the impact of typhoon on  
201 peripheral circulation on sustained ozone enhancement during Typhoon Nepartak through a WRF-chem numerical  
202 simulation.

### 203 3.3 Model simulation and validation

204 To investigate the impact of typhoon periphery and WWD on forming the sustained ozone episode, the numerical model  
205 with the process analysis was applied in this study. Before applying the model to carry out any analysis, the model  
206 performance was validated by using the available observations. Figure S6a-d presents the measured and simulated data  
207 for temperatures, wind speeds, wind directions, and ozone concentrations at Guangzhou from 00:00 on 3 July to 07:00 on  
208 15 July 2016. With regards to the meteorological variables, there was good agreement between the measured and  
209 modelled results, especially the shifting wind features, implying that the model successfully captured the synoptic  
210 features. However, ozone concentrations (Fig. S6d) overestimated low values or underestimated high values some times.  
211 But the simulated results and observed data reasonably agreed with each other and captured the ozone episode in the  
212 region.

213 Statistical metrics including the index of agreement (IOA), mean bias (MB), root mean square error (RMSE), and  
214 normalised mean bias (NMB) were used to further examine the model performance (Table 3). The IOA of the wind  
215 direction was determined according to Kwok et al.(2010), and the IOA values for the other variables were calculated  
216 following the approach of Lu et al.(1997). Generally, our simulation of the time series of ozone concentrations and  
217 meteorological variables was reasonable. All the meteorological parameters were close to the corresponding simulation  
218 results in the PRD region(Wang et al., 2006; Li et al., 2007; Hu et al., 2016). IOAs for temperature and wind speed (0.89  
219 and 0.66, respectively) reached the criteria (as presented in the brackets of Table 3). The model performed well at  
220 capturing the wind directions, with a small MB of 7.72°. MBs and NMBs for temperature and wind speed exceeded the



221 benchmarks; however, they are comparable to the findings of Li et al.(2013) with a slight overestimation, which is  
 222 probably due to the incomplete resolution of the urban morphology impact in the model(Chan et al., 2013). Moreover,  
 223 ozone concentrations are generally well simulated, with an IOA of 0.84 and an NMB of 4.83. Time series comparisons of  
 224 ozone concentrations and meteorological factors at Shenzhen, Zhongshan and Zhuhai are presented in Figs. S6a1-d1,  
 225 a2-d2 and a3-d3. The overall results suggests that the model has the capability to reproduce ozone concentrations and  
 226 capture the transport features in southern China during this period.

227 **Table 3.** Statistical comparison between the observed and simulated variables. The benchmarks are based on  
 228 Emery et al.(2007) and EPA (Doll, 1991). Values that did not reach the criteria are marked in grey.

Variable <sup>a</sup>	IOA <sup>b</sup>	MB <sup>b</sup>	RMSE <sup>b</sup>	NMB <sup>b</sup> (%)
Temp (°C)	0.89 (≥0.8)	0.75 (≤±0.5)	1.90	2.68
Wspd. (m s <sup>-1</sup> )	0.66 (≥0.6)	0.65 (≤±0.5)	1.45 (≤±2.0)	37.81
Wdir. (°)	0.77	7.72 (≤±10)	85.88	4.24
Ozone (ppbv)	0.84	9.53	37.15	4.83 (≤15)

229 <sup>a</sup> Temp. = temperature; Wspd. = wind speed; Wdir. = wind direction.

230 <sup>b</sup> IOA is the index of agreement; MB is the mean bias; RMSE is the root mean square error; NMB is the normalized mean bias.

### 231 **3.4 IPR of the impact of typhoon peripheral circulation on sustained ozone enhancement and** 232 **influence mechanism of WWD on ground-level ozone**

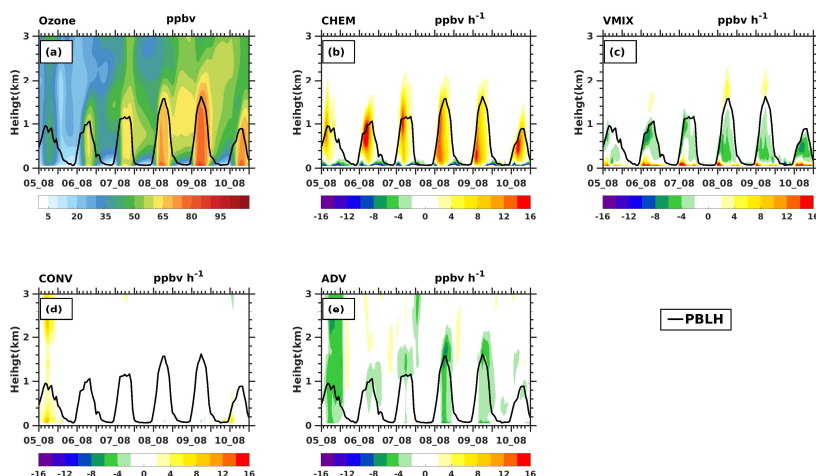
233 As variations in ozone concentration are directly caused by physical and chemical processes(Zhu et al., 2015), the fact  
 234 that peripheral circulation of a typhoon affects ozone concentration can be discussed using an IPR analysis. The  
 235 following processes were taken into account in this analysis: (1) advective transport (ADV) , which is strongly related to  
 236 wind and ozone concentration gradients from upwind areas to downwind areas; (2) vertical mixing (VMIX) caused by  
 237 atmospheric turbulence and vertical gradients of ozone concentrations, which are related to variations in the PBL(Zhang  
 238 and Rao, 1999; Gao et al., 2017); (3) chemistry (CHEM), which is the result of chemical calculations that include ozone  
 239 chemical production and consumption; and (4) convective processes (CONV), i.e. the ozone contribution due to  
 240 convective movements. Complete details on the analytical process of the WRF-Chem model can be found in previous  
 241 studies(J. Gao et al., 2016; H. Zhang et al., 2014) and in the WRF-Chem user guide.

242 Figure 6a shows the profile evolution of the average ozone concentrations in region D0 (black box D0 in Fig. 1) from



243 08:00 on 5 July to 20:00 on 10 July. The ozone concentrations gradually increased from 6 to 9 July throughout the PBL,  
 244 with an increase in PBL height of up to  $\sim 1.5$  km. On 10 July, the PBL height decreased to less than 1 km, and the ozone  
 245 concentrations above 1 km decreased with the PBL; however, the regional average surface ozone concentrations were  
 246 still high but lower than that on 9 July. Figure 6b-e show the vertical distributions of the processes that contribute to the  
 247 ozone concentrations.

248 It can be seen from Fig. 6b-e: during the period from 08:00 to 20:00 on July 5-10, the contributions of CONV in PBL  
 249 were basically zero; CHEM on the ground were strong negative contributions, and VMIX on the ground were strong  
 250 positive contributions; ADV in PBL were weak negative contributions during 6 to 7 July, and the negative contributions  
 251 of ADV in PBL were strengthened on July 8 and 9. Therefore, the contributions of ground VMIX and CHEM played a  
 252 major role in the change of the PBL ozone concentrations, which is consistent with previous studies. At the same time,  
 253 the changes in the strength of ADV contributions in PBL might also have a certain impact on the changes in the ozone  
 254 concentrations on the ground.



255 **Figure 6.** The profile evolution of averaged (a) ozone concentration and (b)-(e) CHEM, VMIX, CONV, and ADV of region D0 from 08:00 5  
 256 July to 20:00 10 July. The black lines denote the planetary boundary layer height(PBLH).

258 In order to investigate the cause of the continued increase of the daytime ozone concentration during the sustained  
 259 ozone episode, the numerical relationship between the daytime average ozone concentration difference of two adjacent



days and the various physical and chemical processes is need to be presented. In the numerical IPR analysis, the ozone concentration at any location at time  $t + 1$  follows Eq. (1):

$$C_{t+1} = C_t + \text{SUM}_{t+1}, \quad (1)$$

where  $C_{t+1}$  and  $C_t$  are the ozone concentrations at time  $t + 1$  and time  $t$ , respectively.  $\text{SUM}_{t+1}$  is the net change in contributions from all of the physical and chemical processes from time  $t$  to time  $t + 1$ , and is shown in Eq. (2):

$$\text{SUM}_{t+1} = \text{ADV}_{t+1} + \text{CHEM}_{t+1} + \text{VMIX}_{t+1} + \text{CONV}_{t+1}. \quad (2)$$

As specified in Eqs. (1) and (2), ozone concentration is a cumulative amount. Then, according to Eq. (1), we obtain:

$$C_{t+24} - C_t = \sum_{j=1}^{j=24} \text{SUM}_{t+j}, (t = 08:00, 09:00, \dots, 20:00), \quad (3)$$

where  $C_t$  and  $C_{t+24}$  are the ozone concentrations at the corresponding time on two adjacent days. For example, if  $C_t$  is the ozone concentration at 8:00 in the morning on a certain day,  $C_{t+24}$  represents the ozone concentration at 8:00 in the next morning.  $\text{SUM}_{t+j}$  is the sum of the contributions from all of the physical and chemical processes at the corresponding time over the time slots. For example, when  $t$  is 08:00,  $\text{SUM}_{08+1}$  indicates the SUM at 9:00 in the morning, and  $\text{SUM}_{08+24}$  indicates the SUM at 8:00 in the next morning. To give the daytime average ozone concentration difference of two adjacent days, we use 08:00 and 20:00 as the daytime and nighttime boundaries to reprocess the hourly data into a half-day average. If the daytime average ozone concentrations for two adjacent days are denoted as  $C_{d1}$  and  $C_{d2}$ , the difference between the daytime average ozone concentrations on two adjacent days can be further expressed by three continuous contribution terms from 09:00 on the first day (d1) to 20:00 on the second day (d2):

$$C_{d2} - C_{d1} = \frac{1}{N} \sum_{t1=09}^{t1=20} (t1-8) \cdot \text{SUM}_{t1} + \sum_{t2=21}^{t2=08} \text{SUM}_{t2} + \frac{1}{N} \sum_{t3=09}^{t3=20} (21-t3) \cdot \text{SUM}_{t3}, \quad (4)$$

where  $C_{d2}$  and  $C_{d1}$  are the daytime average ozone concentrations on two adjacent days.  $N$  is the total number of time slots for the daytime period. Due to the daytime period is between 08:00-20:00,  $N$  is 13. When the right side of Eq. (4)  $> 0$ , the daytime average ozone concentration will increase compared to the daytime average concentration from the previous day, and vice versa. The three terms on the right side of Eq. (4) are referred to as  $\text{SUM}_{d\_d1}$ ,  $\text{SUM}_{n\_d1}$ , and  $\text{SUM}_{d\_d2}$ , respectively.  $\text{SUM}_{d\_d1}$  and  $\text{SUM}_{d\_d2}$  reflect the daytime contributions on two adjacent days.  $\text{SUM}_{n\_d1}$  reflects the



nighttime contribution to difference in daytime average concentration (DDAC) between the two adjacent days. The sum of these three terms is referred to as TOTAL\_SUM. It can be seen from Eq. (4): TOTAL\_SUM is consistent with the evolution of daytime average ozone concentration, that is, when TOTAL\_SUM>0, daytime average ozone concentration increases; when TOTAL\_SUM<0, daytime average ozone concentration decreases. It worthy note that the ozone chemistry between the daytime and nighttime is totally different. The SUM value during daytime is always positive while the SUM of the nighttime is always negative. In terms of the daily daytime variation, the separated three terms illustrate that the daily variation of daytime ozone level not only determined by the daytime increase but also influence by the nighttime ozone variation between the two adjacent day. For example, the nighttime accumulation of ozone (as well as precursors) could also contribute to the daytime ozone increase of the next day. It can be seen from Fig. 7, during the daytime of 6-9 July, TOTAL\_SUM was positive, and the corresponding daytime average ozone concentrations gradually increased; On the 10 July, TOTAL\_SUM was negative, and daytime average ozone concentration began to decrease; However, the daytime SUM on 10 July was still positive. The above analyses indicate that TOTAL\_SUM can well reflect the changing trend of daytime average ozone concentrations, so the cause of the sustained increase in ozone concentrations can be analyzed according to Eq. (4).

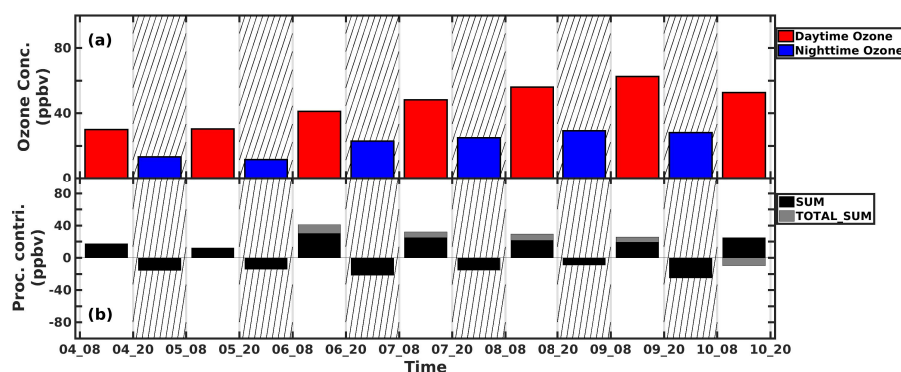


**Figure 7.** (a) daytime and nighttime ozone concentrations and (b) SUM and TOTAL\_SUM on the ground within region D0 during 08:00 4 July to 20:00 10 July

According to Eq. (2), Eq. (4) can be further decomposed into the following form:

$$C_{d2} - C_{d1} = \frac{1}{N} \sum_{t1=09}^{t1=20} (t1-8) \cdot \text{CHEM}_{t1} + \sum_{t2=21}^{t2=08} \text{CHEM}_{t2} + \frac{1}{N} \sum_{t3=09}^{t3=20} (21-t3) \cdot \text{CHEM}_{t3}$$





$$\begin{aligned}
 & + \frac{1}{N} \sum_{t1=09}^{t1=20} (t1-8) \cdot VMIX_{t1} + \sum_{t2=21}^{t2=08} VMIX_{t2} + \frac{1}{N} \sum_{t3=09}^{t3=20} (21-t3) \cdot VMIX_{t3} \\
 & + \frac{1}{N} \sum_{t1=09}^{t1=20} (t1-8) \cdot CONV_{t1} + \sum_{t2=21}^{t2=08} CONV_{t2} + \frac{1}{N} \sum_{t3=09}^{t3=20} (21-t3) \cdot CONV_{t3} \\
 & + \frac{1}{N} \sum_{t1=09}^{t1=20} (t1-8) \cdot ADV_{t1} + \sum_{t2=21}^{t2=08} ADV_{t2} + \frac{1}{N} \sum_{t3=09}^{t3=20} (21-t3) \cdot ADV_{t3} \quad (5)
 \end{aligned}$$

The decomposed items are respectively denoted as:

$$\begin{aligned}
 \text{TOTAL\_SUM\_CHEM} &= \frac{1}{N} \sum_{t1=09}^{t1=20} (t1-8) \cdot \text{CHEM}_{t1} + \sum_{t2=21}^{t2=08} \text{CHEM}_{t2} + \frac{1}{N} \sum_{t3=09}^{t3=20} (21-t3) \cdot \text{CHEM}_{t3}, \\
 \text{TOTAL\_SUM\_VMIX} &= \frac{1}{N} \sum_{t1=09}^{t1=20} (t1-8) \cdot VMIX_{t1} + \sum_{t2=21}^{t2=08} VMIX_{t2} + \frac{1}{N} \sum_{t3=09}^{t3=20} (21-t3) \cdot VMIX_{t3}, \\
 \text{TOTAL\_SUM\_CONV} &= \frac{1}{N} \sum_{t1=09}^{t1=20} (t1-8) \cdot CONV_{t1} + \sum_{t2=21}^{t2=08} CONV_{t2} + \frac{1}{N} \sum_{t3=09}^{t3=20} (21-t3) \cdot CONV_{t3}, \\
 \text{TOTAL\_SUM\_ADV} &= \frac{1}{N} \sum_{t1=09}^{t1=20} (t1-8) \cdot ADV_{t1} + \sum_{t2=21}^{t2=08} ADV_{t2} + \frac{1}{N} \sum_{t3=09}^{t3=20} (21-t3) \cdot ADV_{t3}.
 \end{aligned}$$

Equation (5) shows that the daytime average ozone concentration difference of two adjacent days is determined by

TOTAL\_SUM\_CHEM, TOTAL\_SUM\_VMIX, TOTAL\_SUM\_CONV and TOTAL\_SUM\_ADV.



Table 4. TOTAL\_SUM\_CHEM, TOTAL\_SUM\_VMIX, TOTAL\_SUM\_CONV, and TOTAL\_SUM\_ADV on the ground.

Period (ppbv)	4_08-5_20	5_08_6_20	6_08-7_20	7_08-8_20	8_08-9_20	9_08-10_20
TOTAL_SUM_CHEM	-138.16	-113.817	-133.376	-96.6765	-75.1189	-133.958
TOTAL_SUM_VMIX	118.845	113.4034	131.0915	88.912	70.3796	105.2292
TOTAL_SUM_CONV	33.7043	13.4999	-1.725	0.8075	-2.7115	12.1332
TOTAL_SUM_ADV	-13.9651	-3.3129	10.9665	15.0615	14.0091	6.9084
TOTAL_SUM_CAC	14.3893	13.0863	-4.0095	-6.9570	-7.4508	-16.5956
TOTAL_SUMs	0.4242	9.7734	6.957	8.1045	6.5583	-9.6872

Note: the highlighted column indicate the non-attainment (national-II air quality standard) ozone period. TOTAL\_SUM\_CAC is the sum of the TOTAL\_SUM\_(CHEM+VMIX+CONV).

On the ground, regarding to the daily variability of the daytime ozone levels during the episode, the details budget of the TOTAL\_SUM\_CHEM, TOTAL\_SUM\_VMIX and TOTAL\_SUM\_CONV during the episode are presented in Table 4. More specifically, the CHEM contribution is always negative and VMIX contribution is always positive on the ground which should be the result of the surface NO-titration effect. The CONV contribution is relatively small during the episode (columns highlighted by brown color), while the ADV contribution significantly increased from negative value to positive value from 4 July to 10 July. The TOTAL\_SUMs term is the sum of all the four processes (CHEM+VMIX+CONV+ADV), which show a large daytime ozone enhancement from 5 July to 9 July and a ozone decrease on 10 July. By calculating a sum of CHEM+VMIX+CONV (TOTAL\_SUM\_CAC in the Table 4), we found this three processes changed to negative values during the episode period, while the ADV term changed to positive values and determined the sustained increase of daytime ozone. **The results indicate that both the VMIX and ADV enhancement contributed to the daily increase of daytime ozone concentration from 6 to 9 July on the ground.**

Because the VMIX contribution to the ground is closely dependent on the vertical gradient of the concentration and the turbulence exchange coefficients (Gao et al. 2020) confirm why the VMIX contribution to the surface ozone



reach the maximum (131.0915ppb) from 6 to 7 July, the vertical profiles of accumulative CHEM, ADV, CONV and CAC (CHEM+ADV+CONV) during the time period from 08:00 to 20:00 on 5-7 July are shown in Fig. 8. (For example, the accumulative of CHEM (i.e. the sum of CHEM) from 08:00 to 20:00 on 6 July is denoted as sum of CHEM 06\_08-20). As shown, the gradient of vertical profile of accumulative CHEM contribution on 6 July was significantly larger than that of vertical profiles of accumulative CHEM contribution on 5 July and 7 July (Fig. 8a). The CHEM increase in PBL should be because of the impact of the periphery of Typhoon (Fig. 12a), which would produce a field of meteorological conditions that was conducive to photochemical reactions. These meteorological conditions also led to an increase in the absolute contribution and gradient of accumulative ADV contribution compared to that of 5 July (Fig. 8b). Therefore, the vertical profile gradient of sum of ALL 06\_08-20 was the largest, which contributed to the enhancement of VMIX contribution to the ozone on the ground. In short, both the daytime CHEM and ADV enhancement above the ground throughout the PBL contribute to the increase in VMIX contribution to the ground-level ozone. The CHEM enhancement above the ground should be due to the increase in photochemical formations of precursors within the PBL, while the ADV enhancement above the ground throughout the PBL should be a result of the WWD (weak wind deepening) effect happened in the whole lower troposphere during the episode.

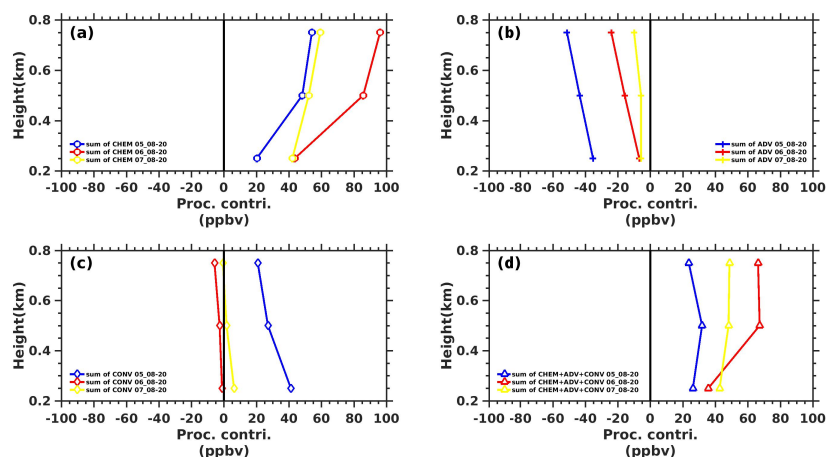


**Figure 8.** The vertical profiles of accumulative (a) CHEM, (b) ADV, (c) CONV, and (d) ALL (CHEM+ADV+CONV) during the periods from 08:00 to 20:00 on 5-7 July.



349       **In summary**, under the impact of the peripheral subsidence of typhoon, the chemical formation (CHEM) and vertical  
350       mixing (VMIX) effects are two major contributors to the enhancement of ozone levels, while the ADV and CONV are  
351       always negative values. But regarding the daily variability of the daytime ozone levels during the episode, the daily  
352       daytime ozone levels do not associated with daily variation of daytime CHEM. By a detail analysis, it is found that the  
353       decrease of the negative ADV throughout the PBL could also play an important role. Results show that the weak  
354       subsidence associated with typhoon periphery provide the premise for the clear sky and warmer air, which is conducive  
355       for the ozone photolysis formation in planetary boundary layer (PBL) above the ground where is dominated by  
356       NO-titration effect. The WWD induced by the peripheral circulation of typhoon system provide the premise for the  
357       enhanced contribution to ozone levels from daily ADV variation throughout the whole PBL, and the increased  
358       contribution to the continue enhancement of ground-level ozone via the VMIX processes.

#### 359       **4. Conclusions**

360       It is widely reported that the peripheral circulation of typhoon favors for the sustained ozone episodes. However, the  
361       process how it impact on the ozone pollution levels during the episodes have not been clearly studied, which is crucial for  
362       better prediction of the daily ozone variation during the episode. In this study, the analysis of ground observation, wind  
363       profile data, and model simulation are integrated. By analyzing the wind profile radar observations, it was found that not  
364       only surface weak winds but also WWD generally appeared in the periphery of Typhoon. The statistics of wind fields and  
365       ground-level ozone at 7 wind profile radar stations in PRD during the 38 typhoons in the Northwestern Pacific Ocean  
366       from 2014-2018 show that the number of WWD occurrences accounts for 93% (87-97%) of the available number of  
367       radar stations for the seven radar stations in average. The number of ozone pollution occurrences accounts for 94% of the  
368       number of WWD occurrences in average. The statistical results show that WWD is a common weather phenomenon in  
369       the periphery of typhoons associated with periphery subsidence of typhoon system and is often accompanied by  
370       significant increases in ozone concentrations.



371 The WRF-chem model was used to simulate the daily daytime ozone variation in a sustained ozone pollution process  
372 in PRD during Typhoon Nepartak in 2016. Validation results show that the model could reasonably reproduce the  
373 observed temperature, wind speed, wind direction and O<sub>3</sub>. Process analysis results show that under the impact of the  
374 peripheral subsidence of typhoon, the chemical formation (CHEM) and vertical mixing (VMIX) effects are two major  
375 contributors to the enhancement of ozone levels, while the ADV and CONV are always negative or small values. But  
376 regarding the daily variability of the daytime ozone levels during the episode, the day-to-day variation of the daytime  
377 ozone levels do not determined by the daily variation of daytime CHEM and VMIX, but the ADV term. By a detail  
378 day-to-day analysis, it is found that the decrease of the negative ADV on the ground and throughout the PBL play an  
379 important role. The integrated effect of the day-to-day variation of the accumulative CHEM above the ground and  
380 accumulative ADV contribution throughout the PBL determined the overall day-to-day daytime ozone variation through  
381 the VMIX process. The enhanced VMIX contribution associated both to the enhanced CHEM and enhanced ADV in the  
382 above PBL.

383 Results show that the weak subsidence associated with typhoon periphery provide the premise for the clear sky and  
384 warmer air, which is conducive for the ozone photolysis formation in planetary boundary layer (PBL) above the ground  
385 where is dominated by NO-titration effect. The WWD induced by the peripheral circulation of typhoon system provide  
386 the premise for the enhanced contribution to ozone levels from daily ADV variation throughout the whole PBL, and the  
387 increased contribution to the continue enhancement of ground-level ozone via the VMIX processes. It shows that the  
388 peripheral characteristics of approaching typhoon not only form the ozone episode by the enhanced photochemical  
389 reactions but also the increase in pollution accumulation throughout the PBL due to the weak wind deepening up to 3~5  
390 km (but not a stability condition in thermodynamics). This result explains why daytime ozone continues to increase,  
391 although the photochemical contribution began to decrease during the event. It also indicate the important role of the  
392 WWD in the lower troposphere for the formation of sustained ozone episodes due to the peripheral circulation of the  
393 typhoon, which helps to better predict the daily changes of daytime ozone levels.

394



395

396

397 *Author contributions.* YL and XZ designed and led the study. JG performed model simulations. XZ and YL analyzed data  
398 and interpreted results. XZ, YL and XD have discussed the results and commented on the paper. XZ wrote the paper with  
399 input from all coauthors.

400

401 *Competing interests.* The authors declare that they have no conflict of interest.

402

403 *Acknowledgements.* We would like to acknowledge the National Centers for Environmental Prediction (NCEP) for the

404 Final Operational Global Analysis data which are freely obtained from the website <https://rda.ucar.edu/datasets/ds083.2/>.

405 The hourly ambient surface O<sub>3</sub> concentration are real-time released by Ministry of Environmental Protection, China on

406 the website <http://www.aqistudy.cn/>, freely downloaded from <http://106.37.208.233:20035/>. The meteorological datas,

407 such as the wind profiler data, automatic weather station data, cloud data and so on, were provided by the China

408 Meteorological Administration and downloaded from <http://172.22.1.175>. This research was supported by the National

409 Natural Science Foundation of China (Grant 41961160728), the Guangdong Province Science and Technology Planning

410 Project of China (Grant 2017A050506003), and Shenzhen Peacock Teams Plan (KQTD20180411143441009).

411

412

413



## 414 ■ References

- 415 Aunan, K., Berntsen, T. K., and Seip, H. M.: Surface Ozone in China and its Possible Impact on  
 416 Agricultural Crop Yields, *AMBIO J. Hum. Environ.*, 29, 294–301, 2000.
- 417 Chan, A., Fung, J. C. H., and Lau, A. K. H.: Influence of urban morphometric modification on regional  
 418 boundary-layer dynamics, *J. Geophys. Res. Atmospheres*, 118, 2729–2747, 2013.
- 419 Chen, X. L., Fan, S. J., Jiang-Nan, L. I., Ji, L., Wang, A. Y., and Soi-Kun, F.: typical weather  
 420 characteristics associated with air pollution in Hong Kong area, *J. Trop. Meteorol.*, 014, 101–104, 2008.
- 421 Chen, Z., Zhuang, Y., Xie, X., Chen, D., Cheng, N., Yang, L., and Li, R.: Understanding long-term  
 422 variations of meteorological influences on ground ozone concentrations in Beijing During 2006–2016.,  
 423 *Environ. Pollut.*, 245, 29–37, 2018.
- 424 Cheng, N. L., Li, Y. T., Zhang, D. W., Chen, T., Wang, X., Huan, N., Chen, C., and Meng, F.:  
 425 Characteristics of Ozone over Standard and Its Relationships with Meteorological Conditions in Beijing  
 426 City in 2014, *Environ. Sci.*, 37, 2016.
- 427 Deng, T., Wang, T., Wang, S., Zou, Y., Yin, C., Li, F., Liu, L., Wang, N., Song, L., and Wu, C. and: Impact  
 428 of typhoon periphery on high ozone and high aerosol pollution in the Pearl River Delta region, *Sci. Total*  
 429 *Environ.*, 668, 617–630, 2019.
- 430 Doll, D. C.: *Guideline for Regulatory Application of the Urban Airshed Model*, 1991.
- 431 Emery, C., Tai, E., and Yarwood, G.: Enhanced meteorological modeling and performance evaluation for  
 432 two texas episodes, in: Prepared for the Texas Natural Resource Conservation Commission, by Environ  
 433 International Corp, 2007.
- 434 Felzer, B. S., Cronin, T., Reilly, J. M., Melillo, J. M., and Wang, X.: Impacts of ozone on trees and crops,  
 435 *Comptes Rendus Géoscience*, 339, 784–798, 2007.
- 436 Feng, Y., Wang, A., Wu, D., and Xu, X.: The influence of tropical cyclone Melor on PM(10)  
 437 concentrations during an aerosol episode over the Pearl River Delta region of China: Numerical modeling  
 438 versus observational analysis, *Atmos. Environ.*, 41, p.4349–4365, 2007.
- 439 Feng, Z., Hu, E., Wang, X., Jiang, L., and Liu, X.: Ground-level O<sub>3</sub> pollution and its impacts on food  
 440 crops in China: A review, *Environ. Pollut.*, 199, 42–48, 2015.
- 441 Forkel, R., Werhahn, J., Hansen, A. B., Mckeen, S., Peckham, S., Grell, G., and Suppan, P.: Effect of  
 442 aerosol-radiation feedback on regional air quality – A case study with WRF/Chem, *Atmos. Environ.*, 53,  
 443 202–211, 2012.
- 444 Gao, J., Zhu, B., Xiao, H., Kang, H., Hou, X., and Shao, P.: A case study of surface ozone source  
 445 apportionment during a high concentration episode, under frequent shifting wind conditions over the  
 446 Yangtze River Delta, China, *Sci. Total Environ.*, 544, 853–863, 2016.
- 447 Gao, J., Zhu, B., Xiao, H., Kang, H., Hou, X., Yin, Y., Zhang, L., and Miao, Q.: Diurnal variations and  
 448 source apportionment of ozone at the summit of Mount Huang, a rural site in Eastern China, *Environ.*  
 449 *Pollut.*, 222, 513–522, 2017.





- 450 Gao, J., Li, Y., Zhu, B., Hu, B., Wang, L., and Bao, f.: What have we missed when studying the impact of  
 451 aerosols on surface ozone via changing photolysis rates?, *Atmospheric Chem. Phys.*, 10831–10844, 2020.
- 452 Giorgi, F. and Meleux, F.: Modelling the regional effects of climate change on air quality, *Comptes*  
 453 *Rendus Geosci.*, 339, 721–733, 2007.
- 454 Grell, G. A., Peckham, S. E., Schmitz, R., McKeen, S. A., Frost, G., Skamarock, W. C., and Eder, B.: Fully  
 455 coupled “online” chemistry within the WRF model, 2005.
- 456 Han, H., Liu, J., Shu, L., Wang, T., and Yuan, H.: Local and synoptic meteorological influences on daily  
 457 variability of summertime surface ozone in eastern China, *Atmospheric Chem. Phys.*, 1–51, 2019.
- 458 Hu, J., Chen, J., Ying, Q., and Zhang, H.: One-Year Simulation of Ozone and Particulate Matter in China  
 459 Using WRF/CMAQ Modeling System, *Atmospheric Chem. Phys. Discuss.*, 16, 10333–10350, 2016.
- 460 Huang, J., Liu, H., Crawford, J. H., Chan, C., Considine, D. B., Zhang, Y., Zheng, X., Zhao, C., Thouret,  
 461 V., and Oltmans, S. J.: Origin of springtime ozone enhancements in the lower troposphere over Beijing: in  
 462 situ measurements and model analysis, 15, 5161–5179, 2015.
- 463 Jiang, Y. C., Zhao, T. L., Liu, J., Xu, X. D., Tan, C. H., Cheng, X. H., Bi, X. Y., Gan, J. B., You, J. F., and  
 464 Zhao, S. Z.: Why does surface ozone peak before a typhoon landing in southeast China?,  
 465 *ATMOSPHERIC Chem. Phys.*, 15, 13331–13338, 2015.
- 466 Kwok, R. H. F., Fung, J. C. H., Lau, A. K. H., and Fu, J. S.: Numerical study on seasonal variations of  
 467 gaseous pollutants and particulate matters in Hong Kong and Pearl River Delta Region, *J. Geophys. Res.*  
 468 *Atmospheres*, 115, 2010.
- 469 Lai, L. Y. and Sequeira, R.: Visibility degradation across Hong Kong: its components and their relative  
 470 contributions, *Atmos. Environ.*, 35, 5861–5872, 2001.
- 471 Li, J., Wang, Z., Akimoto, H., Gao, C., Pochanart, P., and Wang, X.: Modeling study of ozone seasonal  
 472 cycle in lower troposphere over east Asia, *J. Geophys. Res. Atmospheres*, 112, 2007.
- 473 Li, Y., Lau, A. K. H., Fung, J. C. H., Ma, H., and Tse, Y.: Systematic evaluation of ozone control policies  
 474 using an Ozone Source Apportionment method, *Atmos. Environ.*, 76, 136–146,  
 475 <https://doi.org/10.1016/j.atmosenv.2013.02.033>, 2013.
- 476 Li, Y., Lau, A., Wong, A., and Fung, J.: Decomposition of the wind and nonwind effects on observed  
 477 year-to-year air quality variation, *J. Geophys. Res. Atmospheres*, 119, 6207–6220, 2014.
- 478 Lin, X., Yuan, Z., Yang, L., Luo, H., and Li, W.: Impact of Extreme Meteorological Events on Ozone in  
 479 the Pearl River Delta, China, *Aerosol Air Qual. Res.*, 19, 1307–1324,  
 480 <https://doi.org/10.4209/aaqr.2019.01.0027>, 2019.
- 481 Liu, J., Wu, D., Fan, S. J., Liao, Z. H., and Deng, T.: Impacts of precursors and meteorological factors on  
 482 ozone pollution in Pearl River Delta, *Zhongguo Huanjing Kexuechina Environ. Sci.*, 37, 813–820, 2017.
- 483 Lu, R., Turco, R. P., and Jacobson, M. Z.: An integrated air pollution modeling system for urban and  
 484 regional scales: 2. Simulations for SCAQS 1987, *J. Geophys. Res. Atmospheres*, 102, 6081–6098,  
 485 <https://doi.org/10.1029/96JD03502>, 1997.



- 486 Ministry of Ecology and Environment of China: Chinese State of the Environment Bulletin, 1–54, 2016.
- 487 Organization, W. H.: WHO Air quality guidelines for particulate matter, ozone, nitrogen dioxide and  
488 sulfur dioxide - Global update 2005, 2005.
- 489 Shu, L., Xie, M., Wang, T., Gao, D., Chen, P., Han, Y., Li, S., Zhuang, B., and Li, M.: Integrated studies of  
490 a regional ozone pollution synthetically affected by subtropical high and typhoon system in the Yangtze  
491 River Delta region, China, *Atmospheric Chem. Phys.*, 16, 15801–15819, 2016.
- 492 Shu, L., Wang, T., Xie, M., Li, M., Zhao, M., Zhang, M., and Zhao, X.: Episode study of fine particle and  
493 ozone during the CAPUM-YRD over Yangtze River Delta of China: Characteristics and source  
494 attribution, *Atmos. Environ.*, 203, 87–101, <https://doi.org/10.1016/j.atmosenv.2019.01.044>, 2019.
- 495 Skamarock, W. C., Klemp, J. B., Dudhia, J., Gill, D. O., Barker, D. M., Duda, M. G., Huang, X.-Y., Wang,  
496 W., and Powers, J. G.: A Description of the Advanced Research WRF Version 3, 125, n.d.
- 497 Tan, Z., Lu, K., Jiang, M., Su, R., Dong, H., Zeng, L., Xie, S., Tan, Q., and Zhang, Y.: Exploring ozone  
498 pollution in Chengdu, southwestern China: A case study from radical chemistry to O<sub>3</sub>-VOC-NO<sub>x</sub>  
499 sensitivity, *Sci. Total Environ.*, 636, 775–786, 2018.
- 500 Wang, N.: Guangdong Haze Weather Bulletin, 21 pp., 2017.
- 501 Wang, T., Lam, K. S., Lee, A. S. Y., Pang, S. W., and Tsui, W. S.: Meteorological and Chemical  
502 Characteristics of the Photochemical Ozone Episodes Observed at Cape D’Aguilar in Hong Kong, *J. Appl.*  
503 *Meteorol.*, 37, 1167–1178, 1998.
- 504 Wang, T., Wu, Y. Y., Cheung, T. F., and Lam, K. S.: A study of surface ozone and the relation to complex  
505 wind flow in Hong Kong, *Atmos. Environ.*, 35, 3203–3215, 2001.
- 506 Wang, X., Zhang, Y., Hu, Y., Zhou, W., and Russell, A. G.: Process analysis and sensitivity study of  
507 regional ozone formation over the Pearl River Delta, China, during the PRIDE-PRD2004 campaign using  
508 the CMAQ model, *Atmospheric Chem. Phys. Discuss.*, 9, 635–645, 2009.
- 509 Wang, Z., Li, J., Wang, X., Pochanart, P., and Akimoto, H.: Modeling of Regional High Ozone Episode  
510 Observed at Two Mountain Sites (Mt. Tai and Huang) in East China, *J. Atmospheric Chem.*, 55, 253–272,  
511 2006.
- 512 Wu, D., Tie, X., Li, C., Ying, Z., Lau, K. H., Huang, J., Deng, X., and Bi, X.: An extremely low visibility  
513 event over the Guangzhou region: A case study, *Atmos. Environ.*, 39, p.6568-6577, 2005.
- 514 Wu, M., Wu, D., Fan, Q., Wang, B. M., Li, H. W., and Fan, S. J.: Observational studies of the  
515 meteorological characteristics associated with poor air quality over the Pearl River Delta in China,  
516 *Atmospheric Chem. Phys.*, 13, 10755–10766, <https://doi.org/10.5194/acp-13-10755-2013>, 2013.
- 517 Zaveri, R. A. and Peters, L. K.: A new lumped structure photochemical mechanism for large-scale  
518 applications, *J. Geophys. Res. Atmospheres*, 104, 30387–30415, 1999.
- 519 Zaveri, R. A., Easter, R. C., Fast, J. D., and Peters, L. K.: Model for Simulating Aerosol Interactions and  
520 Chemistry (MOSAIC), *J. Geophys. Res. Atmospheres*, 113, 2008.
- 521 Zhang, H., DeNero, S. P., Joe, D. K., Lee, H.-H., Chen, S.-H., Michalakes, J., and Kleeman, M. J.:



- 522 Development of a Source Oriented version of the WRF- Chem Model and its Application to the California  
 523 Regional PM10/PM2.5 Air Quality Study, 20, 2014.
- 524 Zhang, J. and Rao, S. T.: The Role of Vertical Mixing in the Temporal Evolution of Ground-Level Ozone  
 525 Concentrations, *J. Appl. Meteorol.*, 38, 1674–1691, 1999.
- 526 Zhang, J. P., Zhu, T., Zhang, Q. H., Li, C. C., Shu, H. L., Ying, Y., Dai, Z. P., Wang, X., Liu, X. Y., and  
 527 Liang, A. M.: The impact of circulation patterns on regional transport pathways and air quality over  
 528 Beijing and its surroundings, *Atmospheric Chem. Phys.*, 12, 5031–5053, 2012.
- 529 Zhang, Y., Wen, X. Y., and Jang, C. J.: Simulating chemistry-aerosol-cloud-radiation-climate feedbacks  
 530 over the continental U.S. using the online-coupled Weather Research Forecasting Model with chemistry  
 531 (WRF/Chem), *Atmos. Environ.*, 44, p.3568-3582, 2010.
- 532 Zhang, Y., Mao, H., Ding, A., Zhou, D., and Fu, C.: Impact of synoptic weather patterns on  
 533 spatio-temporal variation in surface {O<sub>3</sub>} levels in Hong Kong during 1999–2011, *Atmos. Environ.*, 73,  
 534 41–50, 2013.
- 535 Zhu, B., Kang, H., Zhu, T., Su, J., Hou, X., and Gao, J.: Impact of Shanghai urban land surface forcing on  
 536 downstream city ozone chemistry: URBAN LAND-SURFACE FORCING ON OZONE, *J. Geophys. Res.*  
 537 *Atmospheres*, 120, 4340–4351, <https://doi.org/10.1002/2014JD022859>, 2015.
- 538 Ziomas, I. C., Melas, D., Zerefos, C. S., Bais, A. F., and Paliatatos, A. G.: Forecasting peak pollutant levels  
 539 from meteorological variables, *Atmos. Environ.*, 29, 3703–3711, 1995.

540